Int. j. adv. multidisc. res. stud. 2026; 6(5):1666-1673

Received: 04-09-2026
Accepted: 14-10-2026

International Journal of Advanced Multidisciplinary Research and Studies

ISSN: 2583-049X

Crystal Symmetry and Forbidden Reflections: From Structure Factors to Multiple Diffraction

Konstantinos T Kotsis
Lab of Physics Education and Teaching, Department of Primary Education, University of Ioannina, Greece

DOI: https://doi.org/10.62225/2583049X.2026.6.5.7065
Corresponding Author: **Konstantinos T Kotsis**

Abstract
A diffraction maximum at a nominally forbidden reciprocal-space position does not uniquely identify a reduction in crystal symmetry. Its interpretation depends on the origin of the extinction, the scattering interaction, and the availability of indirect diffraction pathways. This article develops a theoretical and computational account connecting structure-factor cancellation with multiple X-ray diffraction. Lattice-centering absences, restrictions associated with screw axes and glide planes, and cancellations specific to an atomic basis are distinguished before the diamond structure is examined explicitly. In the equal spherical atom approximation, the 222 structure factor vanishes, although allowed secondary and coupling reflections can transfer intensity into the same outgoing direction. A reproducible geometric calculation for a diamond-type cubic model with a = 5.431 Å and λ = 1.5406 Å identifies 180 indexed two-step event branches at 168 distinct azimuths. These are candidate geometries, not predicted intensities or measured peaks. Selected counterexamples demonstrate that vector closure, nonzero coupling factors, and simultaneous elastic conditions must be tested separately. The analysis also explains why true centering absences cannot be filled by successive Bragg transfers within the same ideal translation lattice, whereas basis cancellations can be bypassed. Recent developments in dynamical diffraction software, energy-dependent measurements, and diffuse multiple scattering are considered alongside earlier studies of Umweg peak indexing, polarization, and fine structure. A combined interpretation using azimuth, wavelength, polarization, reciprocal-space shape, and structural consistency provides a defensible basis for evaluating apparent violations of reflection conditions.

Keywords: Crystal Symmetry, Forbidden Reflections, Structure Factors, Multiple X-ray Diffraction, Renninger Effect

Introduction

Crystal symmetry constrains diffraction, but the connection between an observed maximum and a structural conclusion is conditional. An absence predicted by a scalar structure-factor model describes the direct scattering amplitude under that model. A detector measures radiation emerging from a specimen and an optical system, potentially after several coherent scattering events. Accordingly, an unexpected signal can indicate a change in the structure, an incomplete description of the scattering interaction, an indirect pathway, or an instrumental contribution. Distinguishing these possibilities is essential when weak reflections are used to infer a phase transition or to assign a space group.

The term forbidden reflection conceals several physically different situations. A reciprocal point excluded by a translation lattice differs from a reflection canceled by a particular basis. Both differ from a scalar extinction that can be relaxed in an anisotropic resonant scattering channel. Treating these cases as interchangeable produces an especially serious error in the diamond structure: The familiar independent-atom cancellation of 222 is sometimes interpreted as an absolute consequence of the full space group. A more complete electron-density description can permit weak 222 scattering without the proposed symmetry reduction. The classification developed by Dmitrienko *et al.* [1] provides a necessary safeguard against this inference.

Multiple diffraction supplies a second reason for caution. Renninger [2] demonstrated that successive diffraction events can transfer intensity into the outgoing direction of a nominally forbidden reflection, producing pronounced azimuth-dependent maxima. In a two-step pathway, an allowed secondary reflection followed by an allowed coupling reflection reaches the primary outgoing direction even when the direct primary structure factor is zero. Conversely, simultaneous Bragg conditions can redistribute intensity away from an allowed primary reflection. The resulting enhancement, depletion, and interference require wave propagation to be considered alongside structure factors [3]. Subsequent high-resolution studies of silicon have

demonstrated how azimuthal orientation, beam divergence, and wavelength distribution influence the measured profiles [4, 5].

The present article provides a theoretical tutorial supported by an explicitly defined computational example. It is intended for advanced undergraduate and postgraduate students, educators, and researchers seeking a practical connection between reflection conditions and the interpretation of weak diffraction signals. Its contribution is an integrated treatment linking the origin of structure-factor cancellations, the geometric accessibility of indirect scattering pathways, and the evidence required for a symmetry assignment. Established diffraction principles are applied to a diamond-type model to construct an indexed catalogue of elastic two-step candidates. Selected counterexamples demonstrate why vector closure, nonzero coupling factors, and simultaneous elastic accessibility must be checked separately. The catalogue illustrates these distinctions without predicting diffraction intensities or reporting new experimental measurements. The resulting framework supports the critical interpretation of apparent extinction violations and provides a starting point for more complete dynamical calculations.

Structure Factors and the Meaning of an Absence

For elastic scattering from a periodically repeated conventional unit cell, the scalar structure factor can be written using fractional atomic coordinates x_j, occupancies o_j, atomic scattering factors f_j, and displacement factors $\exp(-W_j)$. With integer index vector h = (h, k, l), the adopted phase convention is:

$$F(h) = \Sigma_j o_j f_j \exp(-W_j) \exp(2\pi i\, h \cdot x_j). \quad (1)$$

Far from absorption edges, f_j is often approximated by a spherical independent-atom factor. More generally, scalar anomalous contributions can make it complex. The familiar relation between a kinematical integrated intensity and $|F|^2$ additionally requires polarization, geometric, absorption, volume, and instrumental factors. An observed intensity is therefore not simply a direct reading of Equation (1), especially for nearly perfect crystals under multiple-beam conditions.

A systematic absence is stronger than an accidental small structure factor. A general reflection condition holds for all scattering densities compatible with the relevant symmetry and scattering description. A cancellation at one set of coordinates or occupancies need not survive a physically admissible change in the basis. Numerical smallness also differs from exact cancellation: Finite precision, incomplete coordinate generation, or an arbitrary software threshold can label a weak reflection as forbidden even when no exact symmetry argument requires it.

For a pure translation t relating identical contributions, the phase multiplier is $\exp(2\pi i\, h \cdot t)$. Summing over the centering translations produces a lattice factor. In a conventional face-centered cubic cell, that factor is:

$$L(hkl) = 1 + \exp[\pi i(k + l)] + \exp[\pi i(h + l)] + \exp[\pi i(h + k)]. \quad (2)$$

It equals four when the indices are all even or all odd, and zero for mixed parity. These conditions express the translation lattice itself. A mixed-parity conventional index is not a reciprocal-lattice vector of the face-centered lattice. Equal tensor scatterers related by a pure translation acquire the same phase cancellation, so changing the polarization description alone does not remove a true centering absence.

Screw axes and glide planes combine translations with rotations or reflections. For a simple 2_1 axis along c, two equivalent scalar contributions to 00l differ by $\exp(\pi i l)$, giving 00l only for even l. For a glide translation parallel to a, an analogous restriction can occur for an appropriate reciprocal-space zone. The restriction applies to that zone and symmetry operation; it must not be extended indiscriminately to every hkl. Under resonant tensor scattering, symmetry-related local tensors may be differently oriented, and a scalar screw-axis or glide-plane extinction can have a nonzero polarization-dependent amplitude while the crystal retains its space group [1].

A further category comprises restrictions associated with occupied special positions or a simplified basis. These can disappear when the scattering density is described beyond spherical atoms, even while the space group remains valid. The distinction is particularly relevant to covalent crystals because bonding redistributes electrons away from isolated atomic spheres. A symmetry assignment should therefore specify the reflection condition being tested and the physical model under which that condition is exact.

Diamond Structure and Basis Cancellation

The conventional diamond cell can be described as a face-centered lattice carrying identical atoms at basis positions (0, 0, 0) and (¼, ¼, ¼). Neglecting displacement factors and assigning the same spherical atomic factor f to all eight atoms gives:

$$F(hkl)/f = L(hkl)\{1 + \exp[\pi i(h + k + l)/2]\}. \quad (3)$$

Mixed-parity reflections vanish through L. For all-even indices, the basis factor is zero when h + k + l = 4n + 2 and equals two when the sum is 4n. For all-odd indices the basis factor has magnitude $\sqrt{2}$. Consequently, the normalized intensity $|F/f|^2$ is 64 for the allowed all-even class and 32 for the all-odd class. These values describe an algebraic normalization at each scattering vector; they do not imply that real 400 and 111 intensities have this fixed ratio because their atomic factors and experimental corrections differ.

Table 1 summarizes the lattice and basis contributions for selected reflections in the equal spherical atom diamond model. The 110 reflection vanishes through the face-centered lattice factor, whereas 200 and 222 have nonzero lattice factors but canceled basis contributions. Their identical zero values in this approximation nevertheless have different symmetry implications, as discussed below. The allowed reflections illustrate the normalized squared structure-factor magnitudes for the all-odd and permitted all-even classes. These dimensionless values describe the model's analytical structure factors and should not be

interpreted as measured intensity ratios.

Table 1: Selected structure-factor classes in the spherical diamond model

hkl	L	Basis factor	$\|F/f\|^2$	Reason or class
110	0	0	0	Centering absence
200	4	0	0	Space-group absence for scalar scattering
222	4	0	0	Special-position basis cancellation
111	4	1 − i	32	Allowed all odd
220	4	2	64	Allowed all even
400	4	2	64	Allowed all even

Note: Equal spherical atoms and unit occupancy are assumed. The 222 cancellation need not hold for the complete bonding electron density. Values are normalized at each scattering vector and are not measured intensity ratios

Fig 1 distinguishes the contributions of the translation lattice and the atomic basis. Panel a shows the dimensionless squared structure-factor magnitude, $|F/f|^2$, for selected reflections in the equal spherical atom model. These values describe analytical structure-factor classes rather than measured intensity ratios. For 222, the face-centered lattice factor is four, while the relative basis phase is $\exp(3\pi i) = -1$. Panel b represents the two opposite unit basis phasors; multiplying each by the common lattice factor preserves their cancellation. The resulting zero is exact within the stated model, but it does not require the corresponding Fourier component of the complete bonding electron density to vanish.

Although both 200 and 222 vanish in Equation (3), their cancellations have different symmetry implications. For scalar scattering from an ideal crystal retaining the diamond space group, $Fd\bar{3}m$, the axial reflection condition requires h00 reflections to have h = 4n. Consequently, 200 remains absent even when the electron density is described beyond spherical independent atoms, provided that the density preserves the space-group symmetry. The 222 reflection, by contrast, is not excluded by the general space-group reflection conditions. Its cancellation in Equation (3) follows from the equal spherical atom description of the occupied special positions. Bonding-induced electron-density asphericity or symmetry-compatible anharmonic thermal motion can therefore produce a nonzero 222 structure factor without symmetry lowering [1, 5]. An identical isotropic Debye–Waller factor applied to every atom cannot remove the cancellation because it multiplies the entire structure factor by a common attenuation factor. Thus, a weak direct 222 amplitude can be compatible with the original crystal symmetry, whereas direct scalar 200 scattering requires an explanation beyond that ideal symmetry-preserving density model.

This qualification has practical consequences. A nonzero background-corrected 222 intensity outside an obvious Umweg maximum does not, by itself, establish a subgroup of the diamond space group. Its interpretation requires comparison with a bonding-sensitive electron-density model as well as an appropriate description of instrumental resolution and indirect scattering. A primary study of diamond by Beyer *et al.* [6] illustrates the importance of this distinction: Their synchrotron powder diffraction analysis explicitly accounts for aspherical bonding density and finds harmonic, isotropic thermal motion over the investigated range of 100–1000 K. Bonding-related scattering should therefore not be conflated with evidence for anharmonic motion or symmetry lowering. Although that study concerns carbon diamond rather than silicon, it provides a relevant example of electron-density modeling beyond the spherical independent-atom approximation. For silicon, Zaumseil [5] demonstrates the complementary need to distinguish a persistent 222 contribution from azimuth-dependent multiple-diffraction features.

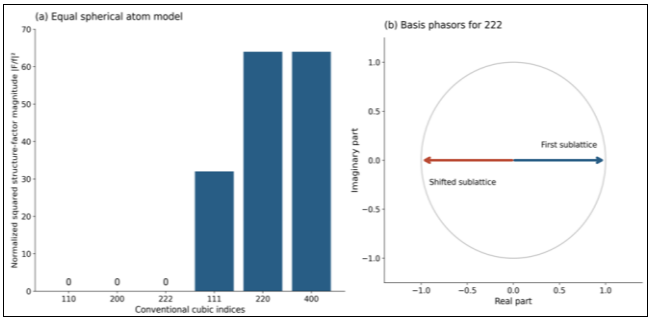

Fig 1: Structure-factor cancellation in the equal spherical atom diamond model: (a) dimensionless squared structure-factor magnitudes for selected reflections; (b) opposite unit basis phasors for 222. Zero values indicate exact cancellations within this approximation

Indirect Pathways and Dynamical Coupling

Let H denote the nominal primary reciprocal vector, Q a secondary transfer, and R = H − Q the coupling transfer. If the incident wavevector is k, a two-step route reaches the same final direction as the direct primary process through k → k + Q → k + H. For an elastic event, the relevant conditions are:

$$|k| = |k + H| = |k + Q| = 1/\lambda, \qquad Q + R = H. \tag{4}$$

Here reciprocal vectors are expressed in inverse-length units without a factor of 2π. With an alternative convention, both reciprocal and wavevector definitions must change together. Equation (4) separates vector closure from simultaneous elastic accessibility. Closure alone does not ensure that the intermediate wave lies on the Ewald sphere.

The leading indirect amplitude contains the product of the secondary and coupling Fourier coefficients. Schematically, a weak-coupling expansion has the form:

$$A(H) \approx A^1(H) + \Sigma Q\, C(H,Q)\, \chi(Q)\chi(H - Q)/D(Q). \tag{5}$$

The susceptibility coefficients χ are proportional to structure factors under consistent conventions. C represents polarization and geometry, while D represents propagation detuning. Equation (5) is a schematic explanation of the available couplings, not a numerical intensity formula. Near an exact multiple-beam condition, a truncated expansion can fail, and the apparent denominator singularity must be replaced by a self-consistent dynamical treatment with boundary conditions, absorption, and finite thickness.

When χ(H) vanishes but χ(Q) and χ(H − Q) do not, the indirect contribution may survive. The outgoing wave then carries the net transfer H without requiring direct first-order scattering by H. If a direct amplitude is present, interference can enhance or diminish the measured signal. Different indirect paths also interfere with one another. Adding independently calculated positive peak intensities discards those phases and cannot generally reproduce the diffraction profile.

Experimental studies demonstrate why peak position, intensity, and profile shape require separate consideration when interpreting multiple diffraction. Consistency between the assumed wavelength and lattice parameters is necessary for reliable indexing of Umweg peaks [7]. Observed fine structure on the Aufhellung side of Renninger peaks also shows that local rocking-curve behavior must be considered when interpreting profile features [8]. Furthermore, Umweg intensities depend on the polarization of the incident beam, so geometric accessibility alone cannot determine the measured intensity [9]. Together, these findings support a distinction between identifying an accessible scattering pathway and predicting its experimental signature. A geometrically indexed event does not specify its strength, and a shoulder or subsidiary maximum should not automatically be assigned to an additional reciprocal-lattice vector.

A useful selection rule follows from translation symmetry alone. The reciprocal lattice of a single ideal crystal is closed under addition. Any sequence of its Bragg transfers therefore remains in that reciprocal lattice. For face-centered conventional indices, adding vectors with uniformly odd or uniformly even parity again yields uniformly odd or uniformly even parity. No such sum produces mixed parity. Thus, repeated allowed Bragg transfers within the same ideal face-centered translation lattice cannot generate a true mixed-parity centering-forbidden reciprocal position. This argument extends to any number of transfers and does not depend on a particular azimuth.

The conclusion has a defined scope. Defects, surfaces, diffuse scattering, overlapping domains, or a second crystal can supply transfers outside the assumed single-lattice Bragg set. Such contributions require an enlarged physical model. Spurious peaks in a multi-crystal spectrometer illustrate why the optical system also matters [10]. This situation should not be described as an ideal single-lattice multiple-diffraction process violating translation symmetry.

Computational Method

The calculation uses a hypothetical ideal diamond-type cell with a = 5.431 Å and λ = 1.5406 Å. These numerical inputs resemble commonly used silicon diffraction conditions, but no particular specimen, temperature, or calibrated instrument is represented. All atoms have equal unit scattering factors; absorption, displacement parameters, tensor scattering, and bonding density are omitted. The output is an elastic-geometry catalogue filtered by the nonzero independent-atom coupling factors.

The primary index is H = (2, 2, 2), and r = λ/a. Define an orthonormal crystal-fixed basis with $e_z = (1, 1, 1)/\sqrt{3}$, $e_x = (1, -1, 0)/\sqrt{2}$, and $e_y = e_z \times e_x$. The incident unit vector u = λk is chosen as:

$$u(\psi) = s(e_x \cos\psi + e_y \sin\psi) - rH/2, \quad s = \sqrt{(1 - r^2|H|^2/4)}. \qquad (6)$$

In Equation (6), H and subsequent integer vectors are dimensionless cubic indices; the physical reciprocal transfer associated with Q is Q/a. This convention gives |u| = |u + rH| = 1 identically. The variable ψ is the incident-direction azimuth in the crystal frame. A laboratory convention based on rotating the crystal can reverse its sign and introduce an arbitrary zero offset. Comparisons of tabulated angles therefore require an explicit coordinate transformation.

The secondary condition becomes a scalar residual,

$$dQ(\psi) = |u(\psi) + rQ|^2 - 1 = A \cos\psi + B \sin\psi + C, \qquad (7)$$

Where $A = 2sr(e_x \cdot Q)$, $B = 2sr(e_y \cdot Q)$, and $C = r^2(|Q|^2 - H \cdot Q)$. For nonzero $\rho = \sqrt{(A^2 + B^2)}$, define $\delta = \mathrm{atan2}(B, A)$. The roots satisfy $\psi = \delta \pm \arccos(-C/\rho)$ modulo 2π, provided $|C/\rho| \leq 1$. If ρ is zero, the residual is constant and must be treated separately; it describes either no event or a continuous geometric condition, rather than two isolated roots.

The candidate search excludes Q = 0 and Q = H and requires both F(Q) and F(H − Q) to be nonzero in the equal-atom model. The triangle inequality applied to Equation (4) gives $|Q| \leq 2/r$. At the stated ratio, each integer component is therefore bounded by seven in magnitude. Searching the cube from −7 to +7 and retaining the spherical bound covers every secondary vector that can lie on the Ewald sphere. No intensity cutoff or assumed peak visibility is used.

A structure-factor tolerance of 10^{-8} in units of f classifies exact analytical zeros represented numerically. The nonzero magnitudes in this model are far above that tolerance. Root-domain values are accepted only within 10^{-12} of the arccos domain, after which clipping corrects roundoff. Distinct azimuths are identified to seven decimal places in degrees. Rounding roots to ten decimal places for tabulation produces a maximum dimensionless elastic residual of approximately 1.2×10^{-12}. These numerical tolerances characterize computation and do not represent experimental angular resolution.

Computational Results

The primary Bragg angle is θ = 29.427845°, giving 2θ = 58.855691°. The complete filtered search identifies 90 distinct secondary vectors Q with nonzero secondary and coupling structure factors and accessible elastic conditions. Each vector produces two distinct azimuthal roots for the stated parameters, yielding 180 indexed event branches. Here, an indexed branch denotes a particular secondary vector paired with one of its elastic roots. After grouping coincident roots using the angular precision specified in the Computational Method, these branches occupy 168 distinct azimuths. Different secondary vectors can therefore satisfy their elastic conditions at the same primary setting. The two roots per vector are a result of this numerical example, rather than a general requirement: Other parameters can produce no root, a tangent root, or a constant residual requiring separate treatment. Neither the branch count nor the number of distinct azimuths predicts the number of experimentally resolved peaks, because coherent coupling, polarization, and instrumental acceptance determine the observable diffraction profile.

Table 2 compares selected two-step routes to the primary 222 direction, illustrating why index closure alone does not establish an accessible diffraction pathway. Although every listed pair satisfies Q + R = H, the route through Q = (1, 1, 1) has no simultaneous elastic solution, whereas Q = (2, 2, 0) has elastic roots but a zero coupling structure factor. The remaining examples satisfy both the structure-factor and elastic requirements and therefore qualify as candidate two-step events. Their calculated azimuths identify geometric settings rather than predict measurable intensities.

Table 2: Closure and elastic accessibility for selected routes to 222

Q	H − Q	|FQ/f|²	|FR/f|²	ψ roots (°)	Two-step status
1 1 1	1 1 1	32	32	None	No elastic root
2 2 0	0 0 2	64	0	0.000000, 180.000000	Zero coupling factor
1 1 3	1 1 -1	32	32	5.723149, 174.276851	Candidate route
1 3 3	1 -1 -1	32	32	90.091996, 329.908004	Candidate route
-1 1 5	3 1 -3	32	32	20.741301, 121.045488	Candidate route

Note: All rows obey index closure. The first two fail different requirements. Candidate routes have nonzero factors and elastic roots; their intensities have not been calculated. Subscripts Q and R label structure factors

The Q = (1, 1, 1) case is an informative counterexample. Its coupling vector is also (1, 1, 1), and both structure factors are nonzero. Nevertheless, the intermediate point lies halfway between the origin and H. At a primary elastic setting it lies inside the Ewald sphere, rather than on its surface. Algebraically, A = B = 0 and C = −3r², which cannot vanish at the chosen wavelength. Index closure and allowed factors therefore do not suffice.

The Q = (2, 2, 0) case fails in a different way. Its secondary elastic equation has roots at 0° and 180°, but R = (0, 0, 2) has zero structure factor in the stated approximation. This route contributes no leading two-step amplitude through the product in Equation (5). It remains possible for an enlarged wave network to populate such an intermediate direction through other allowed couplings. The table classifies a particular two-step route, rather than establishing that every process involving that direction is absent.

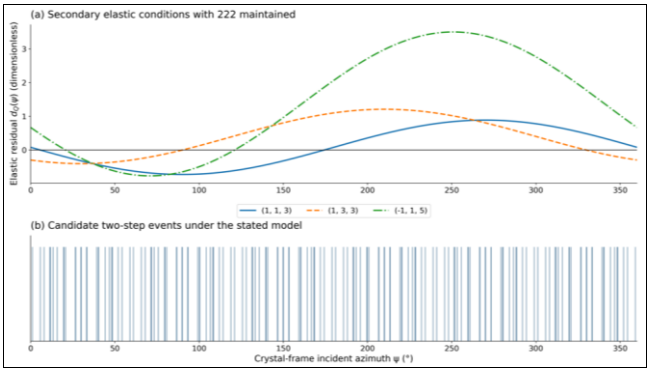

Fig 2: Elastic geometry for H = 222, a = 5.431 Å, and λ = 1.5406 Å: (a) dimensionless secondary elastic residuals; (b) distinct candidate azimuths. Vertical marks represent event positions, not diffraction intensities

For Q = (1, 1, 3), both the secondary and coupling reflections are all odd. The geometric roots are 5.723149° and 174.276851° in the adopted convention. The primary factor remains zero in the spherical equal-atom model, while the two factors controlling the indirect route are nonzero. This is the essential logical content of the classical 222/113 Renninger geometry. High-resolution measurements of this case provide a published experimental context, although the present calculation does not reproduce their dynamical profiles [4].

Fig 2(a) plots the dimensionless elastic residual dQ(ψ) defined in Equation (7) for three selected secondary vectors. Its zero crossings identify azimuths at which the intermediate wave lies on the Ewald sphere while the primary 222 condition is maintained. Fig 2(b) marks the 168 distinct azimuths obtained from the 180 indexed branches; the marks indicate geometric positions and have no intensity meaning. Both panels use the crystal-frame incident-direction convention of Equation (6). Gaps between ideal event positions can guide experimental planning, but they do not establish intervals free from multiple diffraction. Such an assessment additionally requires consideration of wavelength bandwidth, beam divergence, mosaic spread, orientation uncertainty, and pathways beyond the filtered two-step set.

The calculation also shows why an indiscriminate forbidden-reflection filter is unsafe in a general dynamical program. For this particular primary amplitude, the filtered set identifies the nonzero leading two-step products. In a coupled-wave network, a reflection with zero direct structure factor can still be a populated wave channel. Huang and Assoufid [11] explicitly incorporate such detour channels in DXRD. A geometric search intended to seed a full dynamical calculation must therefore retain all relevant wave channels and inspect the couplings between them, rather than delete every nominally forbidden outgoing direction.

Experimental Discrimination and Symmetry Inference

An informative experiment changes conditions that separate competing mechanisms. A Renninger scan maintains the nominal primary condition while varying the azimuth, but its interpretation requires more than identifying a narrow maximum. The wavelength and lattice parameters determine the elastic intersections. Their uncertainty can move an expected event, create an apparent indexing mismatch, or compromise a supposedly clean interval. The concern identified by Alexandropoulos and Kotsis [7] remains relevant when modern calculations are compared with highly monochromatic beams.

Energy variation is especially useful because it changes the Ewald sphere and shifts the multiple-diffraction conditions. It also changes anomalous factors and absorption, particularly near an edge. Nentwich *et al.* [12] address multiple-beam effects in energy-dependent diffraction measurements and methods of avoiding problematic conditions. A feature that moves through an energy–azimuth map can be distinguished from a spectral signal that persists across independently evaluated clean settings. However, energy dependence alone cannot decide between structural and resonant mechanisms because more than one contribution changes with energy.

Polarization analysis supplies a complementary test. The direct tensor amplitude has the form $\varepsilon'^{*}\cdot\hat{F}(H, E)\cdot\varepsilon$, whereas an indirect route includes polarization transformations at successive scattering events. Rotated polarization and harmonic azimuthal dependence can support a resonant tensor interpretation, but multiple diffraction is itself polarization sensitive. The earlier Umweg polarization study by Alexandropoulos and Kotsis [9] is therefore relevant to the design of a control measurement. A polarization signature has to be evaluated against competing models rather than treated as a unique label.

Reciprocal-space mapping helps distinguish a resolution-limited Bragg contribution from extended intensity. Diffuse multiple scattering can generate lines and structured backgrounds, rather than only isolated Umweg maxima. Estradiote *et al.* [13] analyze bright and dark diffuse multiple scattering lines in high-flux experiments. Their work motivates inspecting the two-dimensional or three-dimensional morphology around a weak signal before integrating it as a conventional reflection. The present ideal Bragg catalogue does not model those diffuse contributions.

An additional control concerns wavelength harmonics and optical contamination. A higher-energy component can satisfy a different reflection condition at a detector position interpreted using the nominal wavelength. Measurements using suitable harmonic rejection, verified monochromator settings, and consistent upstream optics can test this possibility. In multi-crystal arrangements, changing one optical component can help determine whether a feature originates in the specimen or in the spectrometer pathway [10]. Such checks are particularly relevant when the weak signal is comparable to the instrument background.

Table 3 summarizes complementary measurements for distinguishing possible origins of intensity at nominally forbidden reflections. Azimuthal and wavelength variation test the accessibility of multiple-diffraction pathways, while polarization analysis and reciprocal-space mapping constrain the scattering mechanism and spatial distribution of the signal. Changes in the optical configuration help identify instrumental contributions, whereas measurements across several reflections and temperatures test the consistency of a proposed symmetry reduction. These comparisons must be interpreted jointly because no single observable uniquely distinguishes structural, resonant, multiple-diffraction, and instrumental contributions.

Table 3: Complementary measurements for interpreting apparent extinction violations

Observable	Relevant comparison	Limit of the inference
Azimuth	Compare peaks and gaps with elastic and dynamical calculations	Finite acceptance can bridge ideal gaps
Wavelength or energy	Track moving multiple-diffraction loci	Absorption and resonant factors also vary
Polarization	Compare direct and indirect channel predictions	Both mechanisms can rotate polarization
Reciprocal-space shape	Resolve a localized spot from extended intensity	Resolution and diffuse scattering require modeling
Optical configuration	Test harmonics and upstream crystal contributions	A changed setting also changes the acceptance
Reflection set and temperature	Fit one symmetry model to several independent observations	Single-peak onset does not establish a subgroup

Note: These comparisons constrain competing explanations jointly. No individual observable uniquely identifies every mechanism

The distinction between structural and multiple-diffraction interpretations has been tested beyond X-ray silicon examples. Sazonov *et al.* [14] compared room-temperature neutron measurements and multiple-diffraction calculations for $Ba_2CoGe_2O_7$, using different wavelengths to distinguish apparent forbidden intensity from genuine symmetry lowering. Their result provides a methodological example of how changing the scattering geometry can revise a structural inference. The neutron interaction differs from X-ray scattering, so its detailed cross sections should not be transferred to the present model; the relevant lesson is the need for discriminating measurements.

A credible symmetry reduction should explain a coherent set of observations. The proposed subgroup must permit the observed reflections, predict compatible intensity relations, and fit the main reflections without creating contradictions. Several independent formerly absent reflections should be measured where indirect scattering has been assessed. A temperature-dependent onset should be checked against thermal changes in lattice parameters, alignment, extinction, and absorption. Otherwise, moving Umweg conditions can mimic an order-parameter-like variation over a limited range.

Statistical treatment should retain background uncertainty and the possibility of zero signal. A small positive integrated count is not automatically evidence for a direct forbidden amplitude. Poisson counting models, measured background regions, and a resolution-convolved forward calculation are preferable to subtracting a smooth baseline and declaring every residual significant. In regions where direct and indirect amplitudes overlap, their interference also prevents a universal additive subtraction of a positive multiple-diffraction intensity. The measurement should support comparison of coherent models rather than rely on a peak-removal recipe.

Discussion

The structure-factor and pathway descriptions answer different questions. The former asks whether the chosen density or susceptibility model contains a direct Fourier component. The latter asks whether coupled waves can produce intensity in a given final direction. Their combination prevents two opposite mistakes: Assigning every nominally forbidden peak to a new structure and assuming every such peak is an experimental artifact. Multiple diffraction is a physical coherent process, and its intensities can carry structural phase information.

Recent computational tools make the connection more accessible. PyDDT links multiple-diffraction calculations with structural refinement through X-ray phase measurements [15]. DXRD extends practical calculations to coupled dynamical waves and finite beam conditions [11]. These developments support a progression from analytical checks to quantitative modeling. They do not remove the need to verify coordinates, reciprocal conventions, scattering factors, and experimental geometry. The simple catalogue presented here is best used to audit geometric assumptions before invoking a more complete solver.

The present model deliberately excludes several mechanisms that matter in quantitative interpretation. Equal unit factors suppress the scattering-vector and energy dependence of real atomic factors. A perfect infinite lattice omits finite-size broadening, strain, surfaces, mosaicity, and defects. The computation tests simultaneous elastic accessibility but does not solve internal wavefields or calculate the response of the receiving optics. It therefore cannot establish which candidate is strongest, how broad it is, or whether a weak symmetry-sensitive contribution would be detectable between candidates.

A further limitation is conceptual rather than numerical. The spherical-atom diamond rule is a convenient reference model, but a question about bonding-sensitive 222 scattering requires a more realistic electron density. Similarly, an experiment near an absorption edge requires tensor susceptibility when anisotropy is significant. Increasing the numerical precision of the spherical calculation cannot supply either missing mechanism. Agreement with a peak position should consequently be treated as evidence for a pathway candidate, while agreement with a symmetry model requires a broader set of intensity and control measurements.

Conclusions

The interpretation of a nominally forbidden reflection requires identification of both the origin of the extinction and the scattering model under which it holds. True centering absences cannot be bypassed by successive Bragg transfers within the same ideal translation lattice. Other cancellations can coexist with accessible indirect pathways, as demonstrated by the diamond-type 222 example. Its counterexamples establish three separate requirements for a leading two-step route: Vector closure, nonzero secondary and coupling factors, and simultaneous elastic accessibility.

A structural inference must extend beyond identifying an accessible pathway or detecting a weak peak. Azimuthal and wavelength variation, polarization analysis, reciprocal-space mapping, and instrumental modeling provide complementary constraints on competing explanations. For 222, the complete bonding electron density must also be considered because a direct amplitude can occur without symmetry lowering. The framework developed here connects analytical reflection conditions to these experimental decisions, while quantitative intensity predictions require a dynamical scattering model appropriate to the specimen and measurement geometry.

Data Availability

No experimental data were collected. The figures and numerical table entries were generated analytically or computationally using the stated model. Supplementary Material S1 provides an executable Python script, the complete catalogue of 180 indexed two-step event branches, and the 168 distinct azimuthal positions with their branch multiplicities. Instructions, model assumptions, numerical tolerances, and verification checks accompany these files. The calculation uses only the Python standard library and does not predict diffraction intensities.

Computational Reproducibility

Generate the eight fractional atomic positions by combining the four centering translations (0, 0, 0), (0, ½, ½), (½, 0, ½), and (½, ½, 0) with the basis positions (0, 0, 0) and (¼, ¼, ¼). Evaluate F(h)/f by summing $\exp(2\pi i\, h\cdot x)$ over these positions. Using $r = \lambda/a$, enumerate integer secondary vectors Q with components from −7 to +7. Retain vectors satisfying $|Q| \leq 2/r$, exclude Q = 0 and Q = H, and apply the structure-factor threshold specified in the Computational Method to both F(Q)/f and F(H − Q)/f.

For each retained vector, calculate A, B, C, and ρ as defined after Equation (7). Treat ρ = 0 separately: A nonzero constant residual gives no elastic event, whereas an identically zero residual represents a continuous condition and must not be counted as two isolated roots. For ρ > 0, apply the stated arccos-domain tolerance and calculate the admissible roots. Count a tangent root once. Convert isolated roots to degrees in [0°, 360°), retain their secondary and coupling indices, and verify each root by direct substitution into the elastic residual. Use unrounded roots for verification, with rounding applied separately for tabulation and identification of coincident azimuths. Preserve the complete indexed list when constructing the separate list of distinct azimuths.

For the stated inputs, these steps yield 90 secondary vectors, 180 indexed branches, and 168 distinct azimuths. These counts provide reference checks for an independent implementation; they do not constitute experimental validation or establish the visibility of individual events.

References

1. Dmitrienko VE, Ishida K, Kirfel A, Ovchinnikova EN. Polarization anisotropy of X-ray atomic factors and “forbidden” resonant reflections. Acta Crystallogr A. 2005; 61(5):481-493. Doi: 10.1107/S0108767305018209
2. Renninger M. „Umweganregung“, eine bisher unbeachtete Wechselwirkungserscheinung bei Raumgitterinterferenzen. Z Phys. 1937; 106:141-176. Doi: 10.1007/BF01340315
3. Batterman BW, Cole H. Dynamical diffraction of X rays by perfect crystals. Rev Mod Phys. 1964; 36(3):681-717. Doi: 10.1103/RevModPhys.36.681
4. Kazimirov A, Kohn VG. High-resolution study of dynamical diffraction phenomena accompanying the Renninger (222/113) case of three-beam diffraction in silicon. Acta Crystallogr A. 2010; 66(4):451-457. Doi: 10.1107/S0108767310010433
5. Zaumseil P. High-resolution characterization of the forbidden Si 200 and Si 222 reflections. J Appl Crystallogr. 2015; 48(2):528-532. Doi: 10.1107/S1600576715004732
6. Beyer J, Grønbech TBE, Zhang J, Kato K, Iversen BB. Electron density and thermal motion of diamond at elevated temperatures. Acta Crystallogr A Found Adv. 2023; 79(1):41-50. Doi: 10.1107/S2053273322010154
7. Alexandropoulos NG, Kotsis KT. Source of misindexing of the Umweg peaks in the Renninger scan. Phys Status Solidi A. 1991; 128(2):K61-6. Doi: 10.1002/pssa.2211280232
8. Alexandropoulos NG, Juretschke HJ, Kotsis KT. Observed rocking-curve fine structure on the Aufhellung side of Renninger-scan peaks. Acta Crystallogr A. 1992; 48(4):490-494. Doi: 10.1107/S0108767392000254
9. Alexandropoulos NG, Kotsis KT. Umweg peak intensity dependence on the incident X-ray beam polarization mode. Solid State Commun. 1994; 89(1):73-75. Doi: 10.1016/0038-1098(94)90421-9
10. Kotsis KT, Alexandropoulos NG. A source of spurious peaks in a multi-crystal X-ray spectrometer. J Phys E Sci Instrum. 1987; 20(1):74-76. Doi: 10.1088/0022-3735/20/1/013
11. Huang X, Assoufid L. DXRD: A user-friendly suite of two- and multiple-beam dynamical X-ray diffraction programs. J Appl Crystallogr. 2025; 58(5):1846-1851. Doi: 10.1107/S1600576725007538
12. Nentwich M, Zschornak M, Weigel T, Köhler T, Novikov D, Meyer DC, *et al*. Treatment of multiple-beam X-ray diffraction in energy-dependent

measurements. J Synchrotron Radiat. 2024; 31(1):28-34. Doi: 10.1107/S1600577523009670
13. Estradiote MB, Nisbet AGA, Penacchio RFS, Miranda MAR, Calligaris GA, Morelhão SL. Simulation of bright and dark diffuse multiple scattering lines in high-flux synchrotron X-ray experiments. J Appl Crystallogr. 2025; 58(3):859-868. Doi: 10.1107/S1600576725003553
14. Sazonov A, Meven M, Roth G, Georgii R, Kézsmárki I, Kocsis V, *et al*. Origin of forbidden reflections in multiferroic $Ba_2CoGe_2O_7$ by neutron diffraction: symmetry lowering or Renninger effect? J Appl Crystallogr. 2016; 49(2):556-560. Doi: 10.1107/S1600576716002405
15. Penacchio RFS, Estradiote MB, Remédios CMR, Calligaris GA, Torikachvili MS, Kycia SW, *et al*. Introduction to Python Dynamic Diffraction Toolkit (PyDDT): Structural refinement of single crystals via X-ray phase measurements. J Appl Crystallogr. 2023; 56(5):1574-1584. Doi: 10.1107/S1600576723005800